

The Assembly of MreB, a Prokaryotic Homolog of Actin*

Received for publication, September 8, 2004, and in revised form, November 12, 2004
Published, JBC Papers in Press, November 16, 2004, DOI 10.1074/jbc.M410298200

Osigwe Esue, Maria Cordero, Denis Wirtz§, and Yiider Tseng¶

From the ‡Department of Chemical and Biomolecular Engineering, The Johns Hopkins University, Baltimore, Maryland 21218

MreB, a major component of the bacterial cytoskeleton, exhibits high structural homology to its eukaryotic counterpart actin. Live cell microscopy studies suggest that MreB molecules organize into large filamentous spirals that support the cell membrane and play a key shape-determining function. However, the basic properties of MreB filament assembly remain unknown. Here, we studied the assembly of *Thermotoga maritima* MreB triggered by ATP *in vitro* and compared it to the well-studied assembly of actin. These studies show that MreB filament ultrastructure and polymerization depend crucially on temperature as well as the ions present on solution. At the optimal growth temperature of *T. maritima*, MreB assembly proceeded much faster than that of actin, without nucleation (or nucleation is highly favorable and fast) and with little or no contribution from filament end-to-end annealing. MreB exhibited rates of ATP hydrolysis and phosphate release similar to that of F-actin, however, with a critical concentration of ~3 nM, which is ~100-fold lower than that of actin. Furthermore, MreB assembled into filamentous bundles that have the ability to spontaneously form ring-like structures without auxiliary proteins. These findings suggest that despite high structural homology, MreB and actin display significantly different assembly properties.

The existence of an extended bacterial cytoskeleton was in doubt until recently. The discovery of intracellular filamentous protein assemblies with cell shape-defining functions has changed our view of the bacterium subcellular organization. In particular, the structural similarities between the protein MreB and its ubiquitous eukaryotic counterpart actin (1) and their similar roles in determining cellular morphology (2–4) suggest that MreB is a structural and functional homolog of actin. The bacterial cytoskeleton also comprises FtsZ, the prokaryotic homolog of tubulin (5), and crescentin, a prokaryotic intermediate filament-like protein (6). Based on homology in amino acid sequences, several bacterial proteins are believed to belong to the actin family. These proteins include the cell division protein FtsA (7), the protein folding chaperone DnaK (8), glucose hexokinase (9), the plasmid DNA segregation pro-

tein ParM (10), as well as the shape-determining filamentous proteins Mb1, and MreB in non-spherical bacterial cells (11–14). Among the known actin-like bacterial proteins, MreB is the most homologous to actin in amino acid sequence, structure, and size (1).

Upon addition of ATP to a MreB solution, MreB molecules polymerize to form single-stranded protofilaments (1), as opposed to actin which forms double-stranded filaments. While the *in vivo* functions of MreB are being actively explored, remarkably little is known about its mechanism of assembly. For instance, it is unknown whether MreB assembly is faster than F-actin¹ assembly given the typically much shorter life-cycle of bacteria compared with mammalian cells. While ATP promotes MreB assembly (1), it is unclear whether MreB catalyzes ATP hydrolysis in a manner similar to F-actin.

Live cell microscopy studies show that MreB molecules assemble into large filamentous spirals that lie under the cell membrane and span the cell length (2–4). When MreB is depleted, rod-shaped *Caulobacter crescentus* cells become lemon-shaped (3) and *Bacillus subtilis* cells become more rounded (2), which both underlie the important mechanical function of MreB (2, 4, 15). In addition to its structural function, MreB is also involved in bacterial chromosomal segregation (16). In eukaryotic cells, the mechanism and regulation of actin assembly as well as F-actin organization into orthogonal arrays and ordered bundles in cytoplasm have been studied extensively (17, 18). However, the assembly mechanism of MreB has yet to be explored.

Because *Thermotoga maritima* is an extreme thermophilic anaerobic eubacteria with optimum growth temperature above 65 °C (19), we investigated the polymerization kinetics of *T. maritima* MreB *in vitro* and determined the basic parameters of its assembly at 65 °C. Using multiple-angle light scattering, we assessed in real time the rigidity and ultrastructure of MreB in solution during assembly. These light scattering studies were complemented by electron microscopy (EM) imaging of MreB filamentous structures. Our studies suggest that MreB filament assembly is not nucleated (or nucleation is highly favorable and fast) and show that MreB polymerizes much more rapidly than actin. Further, these studies suggest that MreB catalyzes ATP hydrolysis and releases phosphate (P_i) at a rate similar to that of F-actin.

MATERIALS AND METHODS

Purification of *T. maritima* MreB—All reagents were purchased from Sigma unless otherwise stated. A pHis17 vector-derived construct containing the *T. maritima* MreB gene was kindly supplied by Dr. Fusinita van den Ent. The purification of *T. maritima* MreB follows van den Ent *et al.* (1) protocol. Briefly, *Escherichia coli* C41(DE3) cells transformed by the MreB gene containing vector were inoculated at 37 °C in 2× YT medium supplemented with 100 µg/ml ampicillin until an OD₆₀₀ of 0.6

* This work was funded by National Science Foundation Grant CTS0210718 and National Aeronautics and Space Administration Grant NAG9-1563. The costs of publication of this article were defrayed in part by the payment of page charges. This article must therefore be hereby marked "advertisement" in accordance with 18 U.S.C. Section 1734 solely to indicate this fact.

§ To whom correspondence may be addressed: Dept. of Chemical and Biomolecular Engineering, The Johns Hopkins University, 3400 N. Charles St., Baltimore, MD 21218. Tel.: 410-516-7006; Fax: 410-516-5510; E-mail: wirtz@jhu.edu.

¶ To whom correspondence may be addressed: Dept. of Chemical and Biomolecular Engineering, The Johns Hopkins University, 3400 N. Charles St., Baltimore, MD 21218. Tel.: 410-516-5287; Fax: 410-516-5510; E-mail: yiider@jhu.edu.

¹ The abbreviations used are: F-actin, filamentous actin; EM, electron microscopy.

and was induced with 1 mM isopropyl- β -D-thiogalactopyranoside for 4 h. The cells were spun down at $6,000 \times g$ for 15 min, quickly frozen in liquid nitrogen, and stored at -20°C for further use. Upon purifying the MreB protein, cell pellets were thawed and resuspended in lysis buffer (50 mM Tris-HCl, pH 8.0, 300 mM NaCl, 1 mM phenylmethylsulfonyl fluoride) containing lysozyme. The mixture was sonicated and DNase I was added. The mixture was centrifuged ($150,000 \times g$) for 1 h, and the supernatant was further purified using a Ni^{2+} -NTA affinity column (Qiagen, Valencia, CA). The column was washed with wash buffer composed of 95% buffer A (50 mM Tris-HCl, pH 8.0, 300 mM NaCl, 1 mM phenylmethylsulfonyl fluoride) and 5% buffer B (50 mM Tris-HCl, pH 6.0, 300 mM NaCl, 1 mM phenylmethylsulfonyl fluoride, and 1 M imidazole), and then eluted with elution buffer composed of 70% buffer A and 30% buffer B. Fractions containing MreB were concentrated and gel-filtrated using Sephacryl S-300 resin (Sigma). The purified protein was dialyzed into polymerization buffer (100 mM Tris-HCl, pH 7.0, 100 mM NaCl) and centrifuged ($150,000 \times g$) for 1 h before use.

Actin Purification and Assembly—Chicken skeletal muscle actin was prepared according to MacLean-Fletcher and Pollard (20) with an added gel filtration step using Sephacryl S-300 (21). Purified actin was continuously dialyzed at 4°C against buffer G (2 mM Tris-HCl, pH 8.0, 0.2 mM ATP, 0.5 mM dithiothreitol, 1 mM sodium azide, and 0.2 mM CaCl_2). Mg^{2+} -actin filaments were generated by adding 0.1 volume of $10\times$ KMEI (500 mM KCl, 10 mM MgCl_2 , 10 mM EGTA, 100 mM imidazole, pH 7.0) polymerizing salt to 0.9 volume of G-actin in buffer G.

Electron Microscopy—MreB was incubated in polymerization buffer (100 mM Tris-HCl, pH 7.0, 100 mM NaCl) with 2 mM ATP at 65°C . For each specimen, 10 μl of the mixture was placed on an electron microscopic grid coated with a collodion film. The grids were washed with three drops of polymerization buffer and stained with 2% uranyl acetate solution. The excess stain was drained off the grid at a 45° angle on a filter paper and dried. Electron microscopy was performed at the Integrated Imaging Center in Johns Hopkins University with a Philips 410 transmission electron microscope at magnification between $\times 65,000$ and $\times 105,000$.

Time-resolved Light Scattering—Time-resolved multiple-angle light scattering (Wyatt Instruments, Santa Barbara, CA) was used to monitor the assembly of MreB and actin. A beam of a 5 milliwatt He-Ne laser (wavelength $\lambda_0 = 632.8$ nm) was incident upon the protein solution contained in a glass vial (sample volume, 5 ml). The background light intensity from the buffer was independently measured and subtracted from the measured light intensities as described previously (22). We report the time-dependent light intensity measured at 90° from the axis of incident light. Protein concentration was varied from 0.05 to 6 μM . All experiments were conducted at 65°C unless otherwise stated. The scattered light intensity was measured simultaneously by 18 photodiodes arranged circularly around the scattering volume. We also report the light intensity, $I(q)$, as a function of the scattering vector amplitude, $q = (4\pi/\lambda_0) \sin(\theta/2)$. The q -dependent scattering light intensity profiles were fitted to a power law $I(q) \sim q^{-a}$. The exponent a reflects the structure of the “scatterers” in solution. The spectrum $I(q)$ is independent of q when the scatterers are much smaller than the length scales probed by the instrument (0.25–1.22 μm). This length scale is larger than individual MreB monomers but smaller than steady state MreB filamentous bundles. However, because extracting morphological information from scattering spectra is an inverse problem (*i.e.* different structures can have the same spectrum $I(q)$), there are typically multiple possible morphologies consistent with a given q -dependent spectrum. Hence, we used time-resolved EM to complement these multiple-angle light scattering measurements.

Phosphate Release Assay—The production of inorganic phosphate by MreB was measured using the malachite green-sodium molybdate assay (23, 24). Polymerization of MreB was initiated by the addition of ATP at 65°C . At 1-min time intervals, the reaction was quenched with one volume of cold 0.6 M perchloric acid and stored on ice until all time points were collected. Two volumes of filtered malachite green solution (0.15 g of malachite green, 1 g of sodium molybdate, 0.25 g of Triton X-100 in 500 ml of 0.7 M HCl) were added to the samples, incubated at room temperature for 30 min, and absorbance measured at OD_{650} using a precision microplate reader (Molecular Devices, Sunnyvale, CA). The curves were normalized with a phosphate standard and a control without protein.

RESULTS

The Polymerization of *T. maritima* MreB Is Temperature-dependent—*T. maritima* performs its biological function in a high temperature environment (19, 25); therefore we studied the

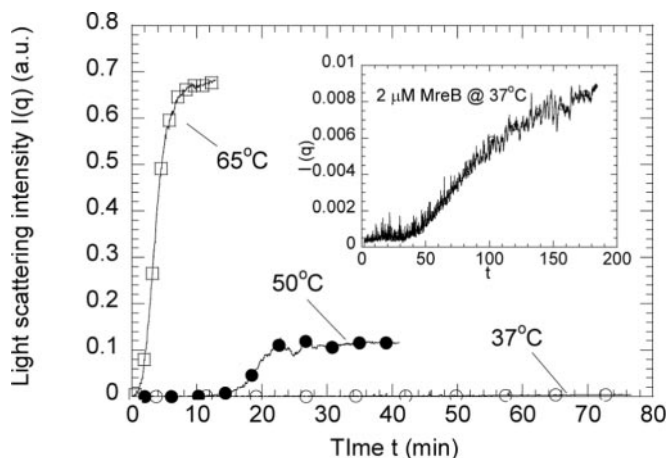


FIG. 1. Temperature-dependent assembly of MreB. Light scattering intensity was monitored at an angle of 90° from the direction of incident light after the addition of ATP to a 2 μM MreB solution. Symbols correspond to 37°C (open circles), 50°C (closed circles), 65°C (open squares). Inset, intensity profile showing the extent of MreB polymerization at 37°C .

effect of temperature on the polymerization of MreB. We monitored the time-dependent intensity of the light scattered from MreB solutions at an angle of 90° and temperatures ranging between 25 and 65°C (Fig. 1). Polymerization was triggered by addition of ATP to MreB solutions (2 μM MreB). At 25°C , we detected no light scattering over the background light scattering from buffer, even 2 h after addition of ATP (data not shown). At 37°C , light scattering increased after a long lag phase of > 40 min and to low intensity levels (Fig. 1, inset). This lag phase was significantly reduced at 50°C and completely eliminated at 65°C (Fig. 1). The steady state scattering intensity at 65°C was ~ 70 times of that at 37°C and the rate of polymerization (as measured by the inverse of the time to reach 90% of the steady state intensity) was much higher at 65°C than at 37°C (Fig. 1). It was essential to determine whether the increase in the rate of MreB polymerization resulted merely from the expected enhanced kinetics of assembly at high temperature. EM showed mostly small amorphous aggregates and very few filamentous structures at 37°C (data not shown). In contrast, at 65°C , EM showed well-developed filamentous bundles (see more below, Fig. 2). Therefore, subsequent MreB experiments were conducted at 65°C , which is within the temperature range for optimal growth of *T. maritima* (19, 25).

MreB Polymerizes and Organizes into Filamentous Bundles—We analyzed the assembly of filamentous MreB as a function of time and concentration, and compared it to the assembly of F-actin. At 65°C , light scattering increased rapidly after addition of ATP, even at an MreB concentration as low as 0.05 μM (Fig. 2A, inset), a concentration at which actin (at 37°C) in polymerization buffer generated no excess scattering above background scattering from buffer. Light scattering showed little or no lag phase at high concentrations (≥ 1 μM) (Fig. 2A), and a short time lag at low concentrations (≤ 1 μM). The extent of this lag was independent of MreB concentration (Fig. 2A, inset). However, the rate of scattering increase and the scattering intensity at steady state increased greatly with MreB concentration (Fig. 2A). For concentrations ≥ 1 μM , MreB polymerization was much faster than actin polymerization, and the scattered light intensity reached a plateau value within minutes (Fig. 2B). Steady state light scattering from polymerized MreB solutions was significantly higher than that from F-actin solutions at the same protein concentration (Fig. 2B and inset).

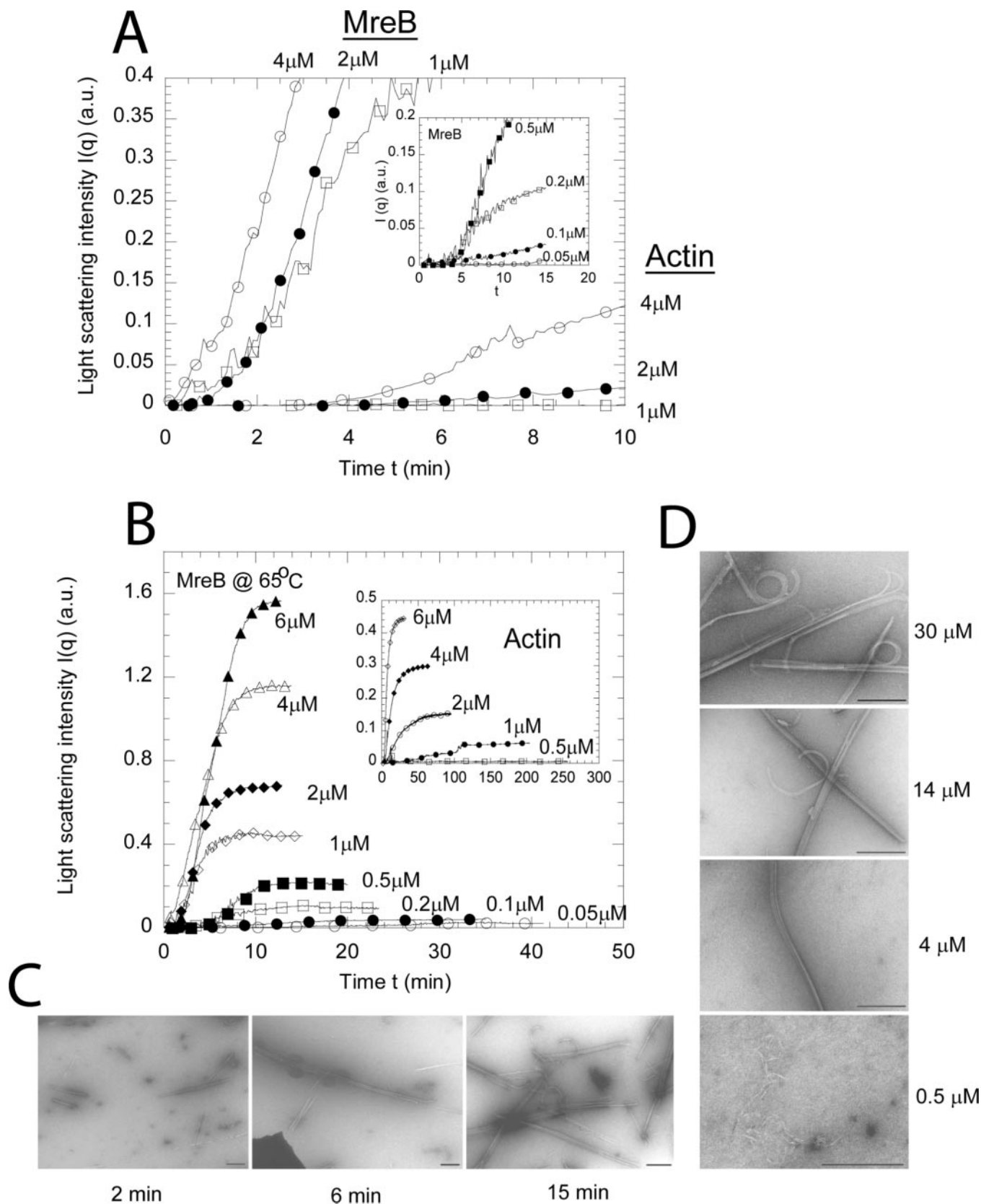


FIG. 2. **Assembly kinetics of MreB.** *A*, time-dependent light scattering intensity for F-actin assembly and MreB assembly at short times. Light scattering was measured at an angle of 90° from the direction of incident light. Symbols correspond to 1 μM (open squares), 2 μM (closed circles), and 4 μM (open circles) for actin and MreB, respectively. *Inset*, intensity versus time for MreB at lower concentrations ($\leq 0.5 \mu\text{M}$) with symbols 0.05 μM (open circles), 0.1 μM (closed circle), 0.2 μM (open squares), and 0.5 μM (closed squares). *B*, time-dependent light scattering intensity for MreB of concentrations varying from 0.05 to 6 μM at long times. *Inset*, intensity versus time for actin at concentrations between 0.5 and 6 μM . *C*, electron micrographs of MreB filaments, taken at 2, 6, and 15 min after the onset of polymerization initiated by adding ATP to a 14 μM MreB solution. *D*, electron micrographs of MreB filaments, taken 15 min after the onset of polymerization by adding ATP into 0.5, 4, 14, and 30 μM MreB solution, respectively. Scale bars, 0.2 μm .

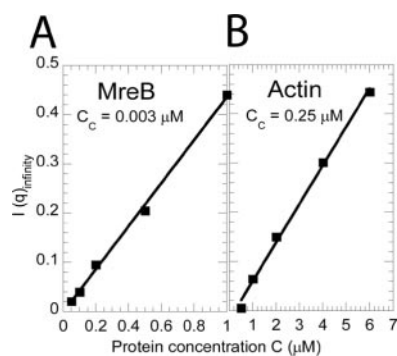


FIG. 3. **Critical concentrations of MreB and F-actin.** Steady state light scattering intensity is plotted as a function of total concentration of protein in solution for A, MreB, and B, actin. The critical concentrations for MreB (~ 3 nM) and actin (~ 0.25 μ M) assembly are estimated by extrapolating the plots to zero intensity.

These light scattering results were complemented by electron micrographs (Fig. 2, C and D). We conducted time-resolved EM at a fixed concentration of 14 μ M MreB. Two minutes after adding ATP, EM revealed that MreB formed short filamentous bundles (Fig. 2C), which increased in length and density with time. After 15 min, MreB filamentous structures consisted of straight and curved bundles as well as closed rings (Fig. 2C). At a fixed elapsed time of 15 min, EM showed that MreB formed mostly single filaments with few thin short bundles at a concentration of 0.5 μ M. At high concentrations, instead of single filaments, thicker and longer filamentous bundles, and rings were observed (Fig. 2D).

The Critical Concentration for MreB Polymerization Is Much Lower Than That of F-actin—To determine the critical concentration required for MreB assembly, the steady state scattering intensity was plotted as a function of the total concentration of MreB in solution (Fig. 3A). An estimate of the critical concentration was obtained by extrapolating this plot to zero intensity. A linear fit of the concentration-dependent intensity suggested a critical concentration of ~ 3 nM. A similar analysis for actin suggested a critical concentration of ~ 0.25 μ M (Fig. 3B), which is between the critical concentrations of its barbed end and pointed end (26).

MreB Catalyzes ATP Hydrolysis—Phosphate release from MreB was investigated to determine whether MreB polymerization is accompanied by ATP hydrolysis (Fig. 4). In the phosphate release assay, a concentration of 100 μ M ATP was used to induce MreB polymerization; thereafter the production of inorganic phosphate was measured at 1-min intervals for a wide range of MreB concentrations (Fig. 4, inset). For MreB concentrations ≥ 1 μ M, the difference in phosphate release between MreB solutions and control solutions without proteins became significant. This phosphate release spectrum suggests that MreB catalyzes ATP hydrolysis. A time lag between phosphate release and MreB polymerization (Fig. 4, inset) suggests that ATP hydrolysis might occur after MreB monomers incorporate into filaments. The rate of phosphate release per mole of MreB was independent of MreB concentration for MreB concentrations ≥ 1 μ M (Fig. 4), with a maximum rate of 0.10 ± 0.01 mol P_i/min/mole MreB (average \pm S.D. of six experiments).

Filament Annealing Does Not Contribute Significantly to MreB Assembly—To determine whether filament end-to-end annealing contributes significantly to overall MreB assembly, the scattering intensity from MreB filament solutions was monitored before and after mechanical shearing (Fig. 5A). When the scattering intensity reached a plateau, the solution was briefly subjected to vigorous shear (Fig. 5A, phase I), and light scattering was immediately re-monitored. As expected, light scattering dropped significantly after shear (Fig. 5A,

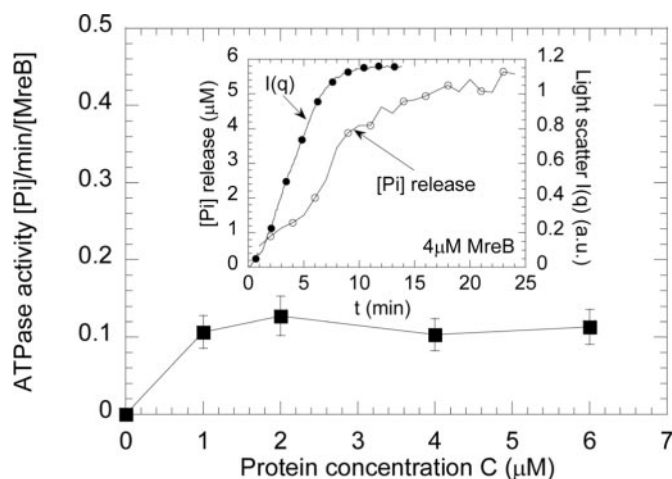


FIG. 4. **ATP hydrolysis monitored by phosphate release during MreB polymerization.** Specific ATPase activity (phosphate release/min/MreB) is plotted as a function of MreB concentration. Inset, light scattering intensity and phosphate release versus time for a 4 μ M MreB solution.

phase II). Filamentous bundles (Fig. 5B, panel I) were broken down to smaller filaments as confirmed by EM (Fig. 5B, panel II). But light scattering failed to recover even in the presence of fresh ATP (Fig. 5A, phase III). The length and structure of the short bundles remained unchanged even 40 min after shear (Fig. 5B, panel III). These results exclude filament end-to-end annealing as a major contributor to MreB assembly. A control experiment was performed with an actin filament solution. For actin, the scattering intensity dropped 50% right after shear but recovered (slowly) to 75% of its original scattering intensity upon addition of ATP (Fig. 5A, inset). This result agrees with previous studies that show that filament end-to-end annealing contributes significantly to actin assembly (27, 28).

MreB Filaments Display Different Morphologies—Real-time morphology of filamentous MreB during assembly was investigated using time-resolved multiple-angle light scattering. The time-dependent scattered light intensities, $I(t; \theta)$, was probed simultaneously by 18 photodetectors placed at different angles, θ , around the glass vial containing the specimen. At a fixed elapsed time after addition of ATP, the apparent rigidity of MreB filamentous structures in solution is indicated by the exponent, α , of the power-law fit of the light scattering profiles, $I(t; q) \sim q^{-\alpha(t)}$. The vector amplitude, q , is defined as $q = (4\pi n/\lambda_0) \sin(\theta/2)$ (see “Materials and Methods”). The predicted exponent for a highly flexible polymer is 2, for which $I(q) \sim q^{-2}$, and 3–4 for sheets and smooth surfaces of three-dimensional objects, for which $I(q) \sim q^{-3}$ or 4 (45). Actin exhibits an exponent of 1.1 (22). The scattered light intensity of polymerized MreB exhibited a q -dependent spectrum (Fig. 6A). At early times, for a wide range of MreB concentrations, the exponent α was ~ 1.5 (Fig. 6B). This suggests that even at early times after initiation of polymerization, MreB formed mostly semi-flexible filaments. At 15 min, the exponent increased to 2.1 for 0.5 μ M, 3.2 for 2 μ M, and 4.0 for 6 μ M, respectively (see “Discussion”).

We complemented these multiple-angle light scattering results with electron micrographs, which showed that MreB organized into filamentous bundles. Sometimes the filamentous bundles became curved, turning into closed ring structures (Fig. 7, A and B). The average thickness of the filamentous bundles in the rings was ~ 4 times the diameter of an MreB filament. This 4-filament thickness could be interpreted as either a 4-filament sheet or a stacked three-dimensional structure of tightly packed filaments. A survey of 112 rings revealed that these rings displayed a relatively uniform diameter of

FIG. 5. MreB filament end-to-end annealing assay. *A*, MreB filament solution polymerized in the presence of ATP (first arrow) to steady state (*I*), is subjected briefly to vigorous mechanical shear (second arrow), and failed to recover even after addition of fresh 2 mM ATP (third arrow). *Inset*, similar study with an actin filament solution, which slowly recovers after shear. *B*, electron micrographs were collected during the three characteristic phases (*I–III*) shown on the intensity profile. *Phases I, II, and III* correspond to the steady state scattering intensity before shear, the intensity right after shear, and the intensity after addition of ATP to the sheared sample, respectively.

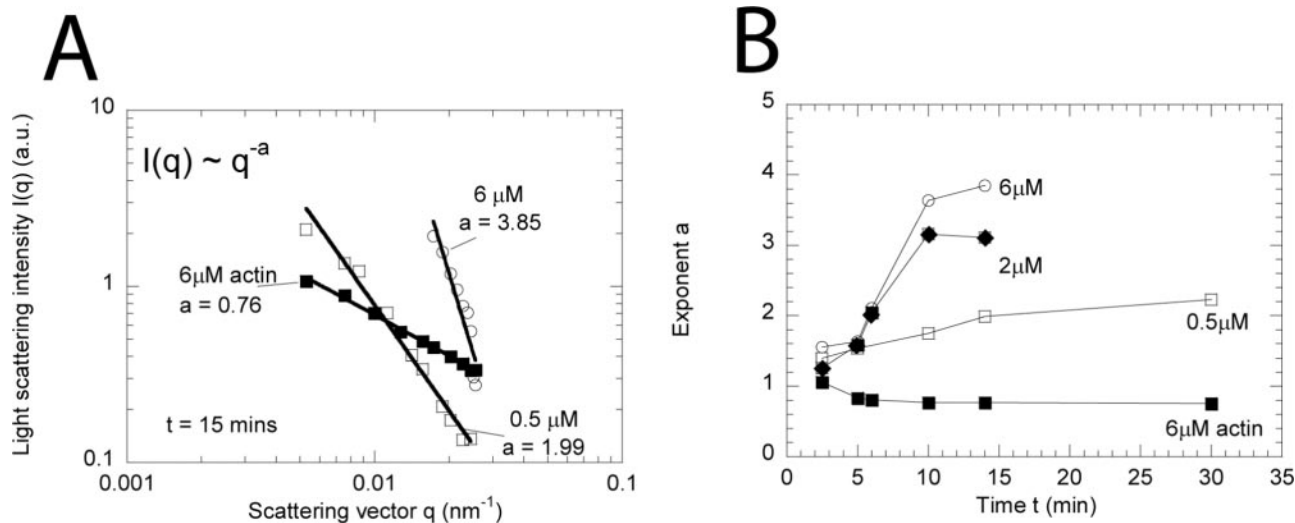
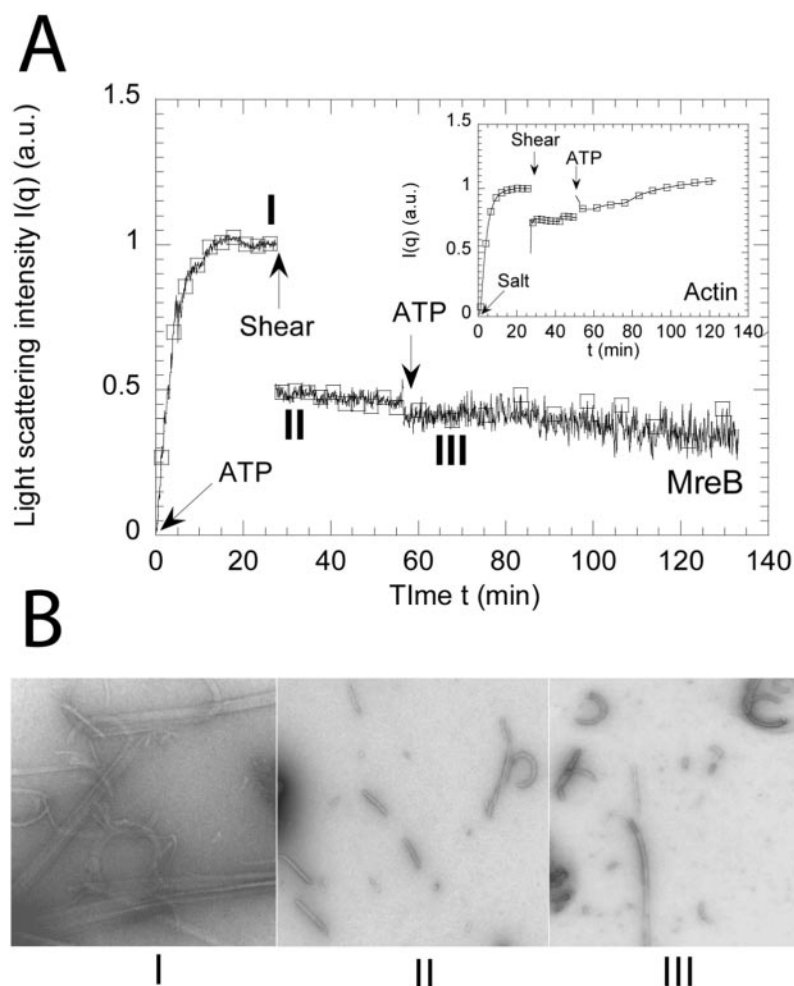


FIG. 6. MreB filament ultrastructure in solution as probed by time-resolved light scattering. *A*, time-dependent exponent a was obtained from power-law fits of scattering spectra $I(t; q) \sim q^{-a(t)}$, such as those shown indicated by the corresponding curves measured 15 min after the onset of MreB polymerization. *B*, time-dependent exponent a for solutions of MreB and F-actin. Symbols in figure correspond to 6 μM F-actin (closed squares), 0.5 μM MreB (open squares), 2 μM MreB (closed circles), and 6 μM MreB (open circles), respectively.

160 \pm 4 nm (mean \pm S.E.) (Fig. 7C).

*The Rate of MreB Polymerization Is Cation-dependent—*Since calcium and magnesium affect greatly the rate and extent of polymerization of actin, we studied the effects of these cations on MreB polymerization (Fig. 8). Calcium slowed down the rate of light scattering increase (Fig. 8A). This cation effect was reproduced in the presence of magnesium ions, except that

there was little difference in the steady state scattering intensity between 1 and 4 mM magnesium (Fig. 8B). The rate of polymerization, defined by the inverse of the time required to reach 90% of the plateau intensity of scattered light, was significantly reduced in the presence of millimolar of either calcium or magnesium (Fig. 8, C and D). Thus, calcium and magnesium decrease the rate of MreB polymerization. Analysis

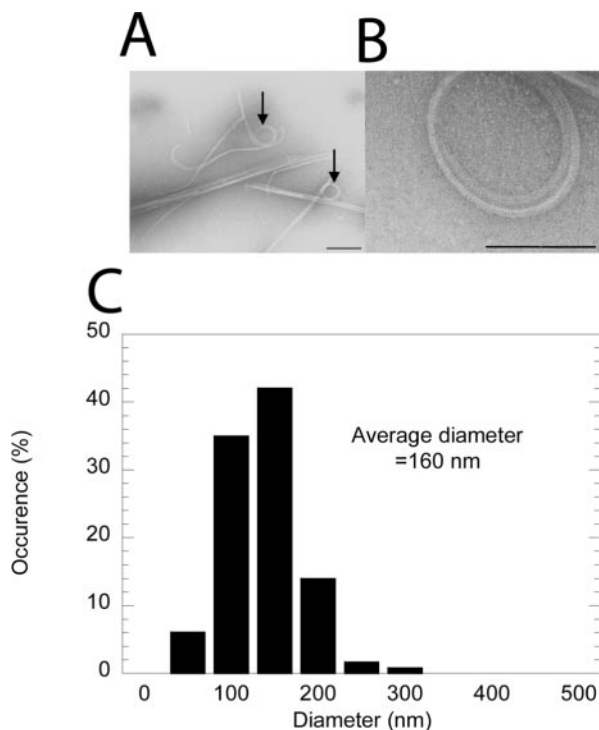


FIG. 7. Ring-like structures of MreB filamentous bundles. *A*, electron micrograph of $14\ \mu\text{M}$ MreB showing filamentous bundles and rings (arrows). Scale bar, $0.2\ \mu\text{m}$. *B*, enlarged ring structure is shown. Scale bar, $0.1\ \mu\text{m}$. *C*, distribution of ring diameters in a sample size of 112 filamentous rings, with a mean of $\sim 160\ \text{nm} \pm 4\ \text{nm}$ (mean \pm S.E.).

of the multiple-angle light scattering showed that, at the same elapsed time (15 min), the power law fit of exponent a of the $I(q)$ profiles in the presence of 1 mM or 4 mM of calcium and magnesium were lower than that in the control solution. At the same scattering intensity (0.5 a.u.), the exponent a was over 2 in the presence of cation ions, whereas that of control solution was below 2. This suggests that the formation of higher ordered MreB filamentous bundles was favored in solutions containing a millimolar range of magnesium or calcium.

DISCUSSION

In this report, the assembly properties, ultrastructure, and ATP hydrolysis of *T. maritima* MreB were studied as a function of concentration and in the absence/presence of calcium and magnesium. To eliminate potential contaminants, MreB was purified through a filtration column after affinity purification. EM and multiple-angle light scattering show that, without accessory proteins, polymerized MreB forms predominantly filamentous bundles. Filament annealing does not contribute significantly to the overall assembly of MreB filaments. Light scattering measurements suggest that the critical concentration for MreB polymerization is $\sim 3\ \text{nM}$, which is ~ 100 times lower than the critical concentration for actin polymerization. Besides filamentous bundles, MreB spontaneously forms ring-like structures with a relatively narrow distribution of radii. In addition, MreB catalyzes ATP hydrolysis, and the phosphate release rate from MreB is comparable to that from F-actin.

MreB Assembly Is Much Faster Than F-actin Assembly—A bacterium contains about 8,000 MreB molecules (2), which corresponds to an intracellular concentration of $0.2\ \text{mg/ml}$ ($5.6\ \mu\text{M}$) *in vivo*. At concentrations around this physiological concentration, we studied *T. maritima* MreB assembly using time-resolved light scattering, an approach used recently to investigate the assembly kinetics of bacterial FtsZ, the prokaryotic homolog of tubulin (24, 29) and ParM, a prokaryotic member of

the actin family (10). We find that the ultrastructure and polymerization kinetics of *T. maritima* MreB depends greatly on temperature. This is not surprising since *T. maritima* is a thermophilic bacterium, with an optimum growth temperature between 65 and $80\ ^\circ\text{C}$ (19, 25). Moreover, enzymes in *T. maritima* show high catalytic activity in the same temperature range (30, 31). At physiological concentrations, *T. maritima* MreB polymerizes significantly more slowly at $37\ ^\circ\text{C}$ than at $65\ ^\circ\text{C}$, with a pronounced lag phase of ~ 40 min.

At $65\ ^\circ\text{C}$, light scattering intensity, which reflects the degree of MreB polymerization, increased almost instantaneously. At low MreB protein concentrations, there appeared to be a short lag that can be explained by the finite sensitivity of our light scattering method, which has a threshold of detection of small polymers ($\sim 20\ \text{nm}$). Indeed, the fact that the lag was independent of MreB concentration (Fig. 2*A*, inset) suggests that this lag is due to the finite sensitivity of the instrument. Together, our results imply that, as opposed to the assembly of its eukaryotic counterpart actin, which involves a nucleation/elongation mechanism, MreB polymerization occurs either without a nucleation phase or with an extremely short-lived, favorable nucleation step.

Bacteria Require a Low MreB Critical Concentration to Perform Their Activities—The critical concentration for MreB polymerization is in the nanomolar range, approximately two orders of magnitudes lower than the critical concentration for actin polymerization. A low critical concentration for MreB assembly suggests a significantly higher affinity both between MreB monomers and between MreB monomer and MreB filament than for actin. It may explain the slightly smaller longitudinal spacing between monomers in a MreB filament ($51\ \text{\AA}$), compared with F-actin ($55\ \text{\AA}$) (1). The much lower intracellular concentration of MreB in bacteria ($5.6\ \mu\text{M}$) compared with actin in eukaryotic cells ($\leq 550\ \mu\text{M}$) (32, 33) may indeed require stronger interactions among MreB to carry out its structural functions compared with actin in eukaryotic cells.

Given the current inaccessibility of a fluorescence assay for MreB assembly, light scattering is the most suitable approach to determine the critical concentration for MreB. As a control, we used light scattering to determine the apparent critical concentration for actin assembly, which has been precisely determined by fluorescence spectroscopy to be $0.1\ \mu\text{M}$ for the slow-growing pointed end and $0.7\ \mu\text{M}$ for the fast-growing barbed end (34, 35). We found that the mean critical concentration for actin is $\sim 0.25\ \mu\text{M}$, between the critical concentrations of the pointed end and the barbed end.

MreB Filaments Increase Their Rigidity by Forming Filamentous Bundles—MreB is critically involved in bacterial morphology and division. A rod-shaped bacterium becomes spherical when MreB is depleted, while *B. subtilis* cells expressing mutated MreB are unable to divide (2–4). As observed by EM, MreB formed filamentous bundles *in vitro*, in agreement with previous studies by Van den Ent *et al.* (1), which is also observed *in vivo* (2). Bundle formation was also indicated by the characteristic values of the exponent a of the q -dependent light scattering spectra (45). A similar upward trend was observed for F-actin solutions in the presence of the F-actin bundling protein fascin (22), for which the exponent a increased with time as filamentous bundles became the dominant structural form. However, it is the opposite in solutions containing only F-actin, for which the exponent a rapidly declines toward unity, the characteristic value of single rigid filaments (22).

Immunofluorescence microscopy showed that MreB forms spirals made of filamentous bundles, which encircle the bacteria cell. These spirals condense into rings at the time of division. The formation of rings may also involve cell division along

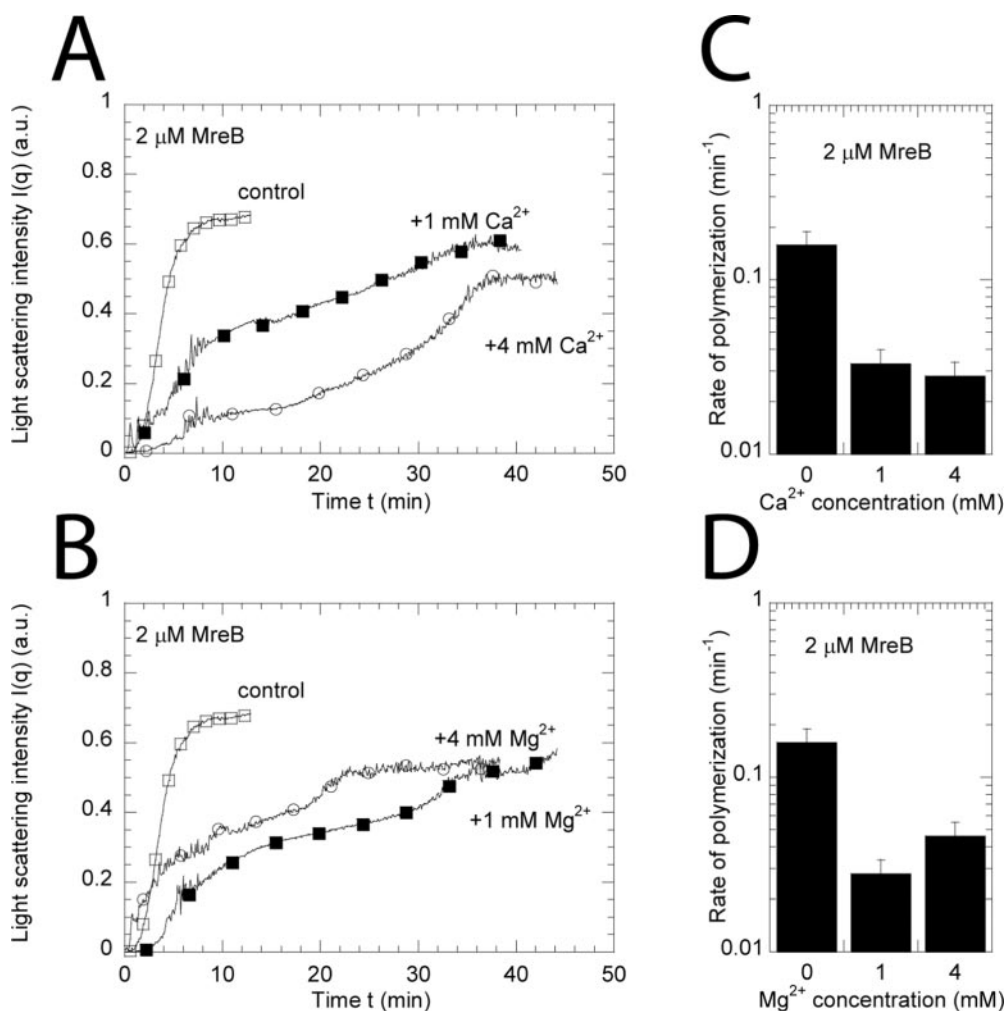


FIG. 8. **Effect of cations on MreB polymerization.** Intensity profiles showed the effect of Ca^{2+} (A) and Mg^{2+} (B). Symbols correspond to a 2 μM MreB solution as a control (open squares), + 1 mM divalent cation (closed squares), and + 4 mM divalent cation (open circles), respectively. In the presence of either Ca^{2+} or Mg^{2+} , the polymerization rates of MreB were slowed down as shown in C and D, respectively. The rate was calculated as the inverse of the time it takes to reach 90% of the steady state light scattering intensity.

with other auxiliary proteins. Here, EM showed that MreB, unlike F-actin and ParM, has the unique potential to spontaneously form rings without auxiliary proteins. Nevertheless, the diameter of rings formed *in vitro* was smaller than observed *in vivo*. Therefore, it is likely that bacteria use auxiliary proteins that cross-link MreB filamentous bundles to the cell membrane to generate a larger spiral diameter.

Comparison Between MreB and Eukaryotic Actin and Prokaryotic ParM—In eukaryotic cells, shape is primarily established and maintained by the actin cytoskeleton. However, despite their cytoplasmic abundance, the F-actin network is not nearly stiff enough to establish cell shape single-handedly (18, 36, 37). This is partly due to the fact that most of cytoplasmic actin remains unpolymerized because actin-sequestering proteins regulate and maintain a large pool of monomeric actin. Eukaryotic cells cope with this problem by exploiting cross-linking/bundling proteins, such as α -actinin and filamin, to organize actin filaments into stiff, yet dynamic arrays (38, 39). It was believed that, in bacteria, shape was mostly established by the peptidoglycan-rich cell wall (2). However, recent work shows that MreB and Mbl play a major role in controlling the shape of bacterial cells (2, 3). Regulation of cell shape by MreB may come in two ways. MreB filaments may bind factors that are released upon MreB disassembly, which affect the organization and mechanics of the cell wall or, more likely, MreB filament structures themselves may contribute greatly to cell

mechanics. Our results showed that MreB filaments form thick bundles without the presence of auxiliary proteins. These filamentous bundles appeared more rigid than eukaryotic F-actin or bacterial ParM filaments (29). Based on our EM observations and in analogy to ParM, which is stabilized by the ParC-ParR complex during DNA segregation (40), it is likely that MreB filaments also required auxiliary cross-linking factors to reinforce the stiff cortex-like structures observed in bacteria and to anchor these assemblies to the cell membrane.

EM showed that MreB spontaneously forms filamentous bundles *in vitro*. Short bundles were present at early times during assembly; as time progresses, these filamentous bundles elongated. Our results also show that like most other biopolymers, MreB polymerization occurred by addition of monomers to filament ends. Attempts to break the filaments and have them anneal without auxiliary proteins were unsuccessful. Light scattering from sheared MreB filaments remained constant for a long time, even after addition of ATP, which indicated the absence of filament end-to-end annealing or re-polymerization. In contrast, light scattering confirmed that broken actin filaments can anneal (slowly) (27). Whether end-annealing is unique to F-actin and is not displayed by other actin-like proteins in bacteria is an interesting question to address. However, annealing of filamentous ParM during assembly may be difficult to assess experimentally as it disassembles immediately upon ATP hydrolysis (13, 41).

For cytoskeletal proteins such as actin (42) and ParM (10), ATP hydrolysis closely follows polymerization. Interestingly, the release of hydrolyzed phosphate appears to lag slightly behind *T. maritima* MreB polymerization, similar to ATP hydrolysis on F-actin from its pointed end (42). The rate of phosphate dissociation from MreB ($\sim 0.10 P_i$ per actin per min) was seemingly slower than from ParM ($\sim 2.5 P_i$ per ParM per min, Ref. 10), but similar to that from F-actin ($\sim 0.16 P_i$ per actin per min, Ref. 43). This may be due to the fact that the nucleotide binding sites of MreB and actin are similarly located near the base of the cleft between domains I and II (1).

In dividing eukaryotic cells, F-actin localizes to mid-cell to form the actin-myosin contractile ring (44). In bacteria, MreB is mostly localized right under the cell membrane and similarly moves to the cell mid-point at the time of cell division (3). This switch in subcellular localization of MreB requires MreB filaments to be dynamic *in vivo*, which is consistent with our observations *in vitro*. At physiological concentrations, MreB polymerized within ~ 2 – 3 min, a time commensurate with physiological time scales (e.g. *E. coli* has a cell cycle ~ 30 min). MreB ability to polymerize rapidly would allow MreB to perform effectively its cell-shape defining function after the formation of the two daughter cells.

The current analysis does not allow us to determine some of the details of the mechanism of MreB polymerization. In particular, the determination of the critical concentrations for both ends of MreB will have to wait for the identification of capping proteins that selectively block the growth of MreB filaments at both ends.

Acknowledgments—We thank Dr. Fusinita van den Ent for kindly providing us with the full-length cDNA of *T. maritima* MreB, Michael McCaffery at the Integrated Imaging Center for technical assistance with EM, and Dr. Michael Ostap for useful discussions.

REFERENCES

- van den Ent, F., Amos, L. A., and Lowe, J. (2001) *Nature* **413**, 39–44
- Jones, L. J., Carballido-Lopez, R., and Errington, J. (2001) *Cell* **104**, 913–922
- Figge, R. M., Divakaruni, A. V., and Gober, J. W. (2004) *Mol. Microbiol.* **51**, 1321–1332
- Daniel, R. A., and Errington, J. (2003) *Cell* **113**, 767–776
- Bi, E. F., and Lutkenhaus, J. (1991) *Nature* **354**, 161–164
- Ausmees, N., Kuhn, J. R., and Jacobs-Wagner, C. (2003) *Cell* **115**, 705–713
- van den Ent, F., and Lowe, J. (2000) *EMBO J.* **19**, 5300–5307
- Itoh, T., Matsuda, H., and Mori, H. (1999) *DNA Res.* **6**, 299–305
- Holmes, K. C., Sander, C., and Valencia, A. (1993) *Trends Cell Biol.* **3**, 53–59
- Moller-Jensen, J., Jensen, R. B., Lowe, J., and Gerdes, K. (2002) *EMBO J.* **21**, 3119–3127
- Carballido-Lopez, R., and Errington, J. (2003) *Dev. Cell* **4**, 19–28
- Soufo, H. J., and Graumann, P. L. (2003) *Curr. Biol.* **13**, 1916–1920
- Moller-Jensen, J., Borch, J., Dam, M., Jensen, R. B., Roepstorff, P., and Gerdes, K. (2003) *Mol. Cell* **12**, 1477–1487
- van den Ent, F., Moller-Jensen, J., Amos, L. A., Gerdes, K., and Lowe, J. (2002) *EMBO J.* **21**, 6935–6943
- Wachi, M., and Matsuhashi, M. (1989) *J. Bacteriol.* **171**, 3123–3127
- Kruse, T., Moller-Jensen, J., Lobner-Olesen, A., and Gerdes, K. (2003) *EMBO J.* **22**, 5283–5292
- Heidemann, S. R., and Wirtz, D. (2004) *Trends Cell Biol.* **14**, 160–166
- Kole, T. P., Tseng, Y., Huang, L., Katz, J. L., and Wirtz, D. (2004) *Mol. Biol. Cell* **15**, 3475–3484
- Londei, P., Altamura, S., Huber, R., Stetter, K. O., and Cammarano, P. (1988) *J. Bacteriol.* **170**, 4353–4360
- MacLean-Fletcher, S. D., and Pollard, T. D. (1980) *J. Cell Biol.* **85**, 414–428
- Tseng, Y., An, K. M., and Wirtz, D. (2002) *J. Biol. Chem.* **277**, 18143–18150
- Tseng, Y., Fedorov, E., McCaffery, J. M., Almo, S. C., and Wirtz, D. (2001) *J. Mol. Biol.* **310**, 351–366
- Geladopoulos, T. P., Sotiroidis, T. G., and Evangelopoulos, A. E. (1991) *Anal. Biochem.* **192**, 112–116
- Romberg, L., Simon, M., and Erickson, H. P. (2001) *J. Biol. Chem.* **276**, 11743–11753
- Hecht, K., Wrba, A., and Jaenicke, R. (1989) *Eur. J. Biochem.* **183**, 69–74
- Nishida, E., and Sakai, H. (1983) *J. Biochem. (Tokyo)* **93**, 1011–1020
- Murphy, D. B., Gray, R. O., Grasser, W. A., and Pollard, T. D. (1988) *J. Cell Biol.* **106**, 1947–1954
- Andrianantoandro, E., Blanchoin, L., Sept, D., McCammon, J. A., and Pollard, T. D. (2001) *J. Mol. Biol.* **312**, 721–730
- Mukherjee, A., and Lutkenhaus, J. (1999) *J. Bacteriol.* **181**, 823–832
- Lee, D. W., Jang, H. J., Choe, E. A., Kim, B. C., Lee, S. J., Kim, S. B., Hong, Y. H., and Pyun, Y. R. (2004) *Appl. Environ. Microbiol.* **70**, 1397–1404
- Hecht, K., Langer, T., Wrba, A., and Jaenicke, R. (1990) *Biol. Chem. Hoppe. Seyler.* **371**, 515–519
- Pollard, T. D., and Cooper, J. A. (1986) *Ann. Rev. Biochem.* **55**, 987–1035
- Pollard, T. D., Blanchoin, L., and Mullins, R. D. (2000) *Annu. Rev. Biophys. Biomol. Struct.* **29**, 545–576
- Cooper, J. A., and Pollard, T. D. (1985) *Biochemistry* **24**, 793–799
- Weber, A., Pennise, C. R., Babcock, G. G., and Fowler, V. M. (1994) *J. Cell Biol.* **127**, 1627–1635
- Yamada, S., Wirtz, D., and Kuo, S. C. (2000) *Biophys. J.* **78**, 1736–1747
- Kole, T. P., Tseng, Y., Jiang, I., Katz, J. L., and Wirtz, D. (2004) *Mol. Biol. Cell to appear*
- Tseng, Y., An, K. M., Esue, O., and Wirtz, D. (2004) *J. Biol. Chem.* **279**, 1819–1826
- Tseng, Y., Schafer, B. W., Almo, S. C., and Wirtz, D. (2002) *J. Biol. Chem.* **277**, 25609–25616
- Jensen, R. B., and Gerdes, K. (1999) *EMBO J.* **18**, 4076–4084
- Jensen, R. B., and Gerdes, K. (1997) *J. Mol. Biol.* **269**, 505–513
- Blanchoin, L., and Pollard, T. D. (2002) *Biochemistry* **41**, 597–602
- Carlier, M. F., and Pantaloni, D. (1986) *Biochemistry* **25**, 7789–7792
- Li, F., Wang, X., Bunger, P. C., and Gerdes, A. M. (1997) *J. Mol. Cell Cardiol.* **29**, 1541–1551
- Higgins, J. S., and Benoit, H. C. (1994) *Polymers and Neutron Scattering*, pp. 141–191, Oxford University Press, Oxford